Available online at www.sciencedirect.com

ScienceDirect

Energy Procedia 63 (2014) 997 – 1017

Energy Procedia

GHGT-12

# Thermodynamic modeling of aqueous piperazine/N-(2-aminoethyl) piperazine for $CO_2$ capture

Yang Du[a], Gary T. Rochelle[a,*]

[a]McKetta Department of Chemical Engineering, The University of Texas at Austin, 200 E Dean Keeton St. Stop C0400, Austin, TX 78712-1589, USA

**Abstract**

Aqueous piperazine (PZ) blended with N-(2-aminoethyl) piperazine (AEP) is an attractive solvent for $CO_2$ capture from coal-fired power plants. A rigorous thermodynamic model was developed in Aspen Plus® to predict properties of PZ/AEP/$H_2O$/$CO_2$, using the electrolyte-Nonrandom Two-Liquid (eNRTL) activity coefficient model. A sequential regression was performed to represent $CO_2$ solubility, speciation, and amine volatility data over operationally significant loading and temperature ranges. The model predicts a $CO_2$ cyclic capacity of 0.86 mol/kg (PZ + AEP + water) for 5 m PZ/2 m AEP, compared to 0.50 mol/kg for 7 m MEA and 0.86 mol/kg for 8 m PZ. The predicted heat of absorption is 75 to 85 kJ/mol $CO_2$ in the operating loading range (0.288–0.380 mol $CO_2$/mol alkalinity). Speciation for PZ/AEP/$H_2O$ at various $CO_2$ loading and temperature was also predicted, from which behavior of $CO_2$ in the amine system was proposed.



Peer-review under responsibility of the Organizing Committee of GHGT-12

*Keywords:* Piperazine; Aminoethylpiperazine; $CO_2$ capture; eNRTL; Modeling

## 1. Introduction

Amine scrubbing has shown the most promise for effective capture of $CO_2$ from coal-fired flue gas [1]. However, with traditional amine solvents such as monoethanolamine (MEA), the energy penalty for solvent regeneration and $CO_2$ compression is prohibitive. Concentrated piperazine (PZ) has been proposed as a better solvent for $CO_2$ capture from coal-fired flue gas, with a 10% energy benefit compared to MEA [2,3]. The application of concentrated PZ is

* Corresponding author. Tel.: 1-512-471-7230; fax: 1-512-471-7060.
*E-mail address:* gtr@che.utexas.edu


Peer-review under responsibility of the Organizing Committee of GHGT-12
doi:10.1016/j.egypro.2014.11.108

limited by its low solubility in water at low temperature and lean $CO_2$ loading [3]. Blending less concentrated PZ with its structural analog N-(2-aminoethyl) piperazine (AEP) remediates the precipitation issue while conserving the most desirable characteristics of concentrated PZ [4].

To predict the overall performance of this amine blend, it is necessary to develop a rigorous thermodynamic model which can accurately predict the thermodynamic properties, specifically vapor-liquid equilibrium (VLE), calorimetric properties, and chemical reaction equilibrium.

The thermodynamic properties of a variety of aqueous amine solutions for $CO_2$ absorption have been successfully modeled with the electrolyte-Nonrandom Two-Liquid (eNRTL) model as a thermodynamic framework. Austgen [5] used the eNRTL model developed by Chen and coworkers [6] to model the VLE of carbon dioxide over aqueous N-methyl-diethanolamine (MDEA), monoethanolamine (MEA), diethanolamine (DEA), and Diglycolamine® (DGA®). Posey [7] improved the Austgen models by studying the activity coefficient of the amines at infinite dilution. An activity-based PZ-$H_2O$-$CO_2$ model was developed by Hilliard [8] in Aspen Plus®. Frailie [9] extended Hilliard's model to represent various thermodynamic properties of more concentrated PZ solutions and identified this model as the Independence model.

In this work, a thermodynamic model for PZ-AEP-$H_2O$-$CO_2$ system was developed in Aspen Plus® based on the Independence model [9]. Unavailable model parameters were obtained by regressing experimental data, or by reference to the Independence model results for PZ. Amine volatility and $CO_2$ solubility data were used in regression. NMR measurements were used to validate the model prediction of aqueous speciation distribution. Heat of absorption for this solvent was predicted at operating conditions.

## 2. Thermodynamic framework

The thermodynamic model built for PZ-AEP-$H_2O$-$CO_2$ in this work is based on the model for PZ-$H_2O$-$CO_2$ ("Independence" model) developed by Frailie [9] in Aspen Plus®. Therefore, the basic thermodynamic framework is identical to the Independence model: using the eNRTL model for liquid phase behavior and the Soave-Redlich-Kwong (SRK) equation for gas phase behavior.

### *2.1. Aqueous-Phase Chemical Equilibrium*

AEP is a tri-amine with primary, secondary, and tertiary amine groups in its structure, leading to various protonated and carbamate species. The third pKa of AEP was reported to be below 4 at 25–50 °C [10], while the normal pH value in $CO_2$-loaded amine solution at the rich loading is typically well above 8. Therefore, the amount of tri-protonated AEP is extremely small in loaded solutions and it is excluded from consideration in this work. Both the primary and secondary amino groups of AEP can connect with a carboxyl group, leading to two isomers of AEP carbamate. Table 1 lists potential species in PZ-AEP-$H_2O$-$CO_2$. For simplicity, protonated species are not listed. To differentiate the carbon nuclei with different electronic environments, they are numbered for different species present.

Table 1. Molecular structure of the compounds in $CO_2$-loaded PZ-AEP aqueous solutions

| Name | Molecular Structure |
|---|---|
| AEP | 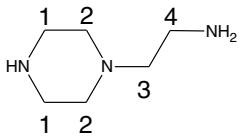 |

| | |
|---|---|
| $AEPCOO^-$ | 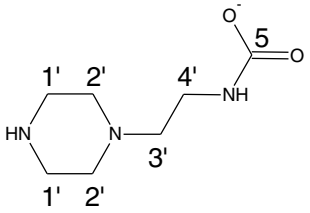 |
| $^-OOCAEP$ | 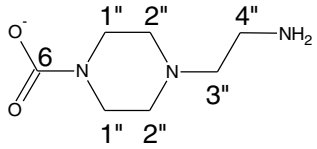 |
| $AEP(COO^-)_2$ | 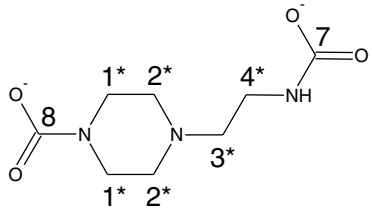 |
| PZ | 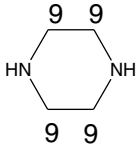 |
| $PZCOO^-$ | 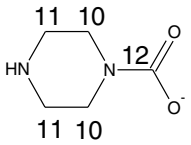 |
| $PZ(COO^-)_2$ | 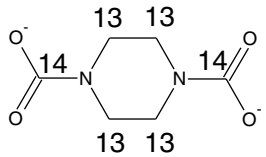 |
| $HCO_3^-/CO_3^{2-}$ | 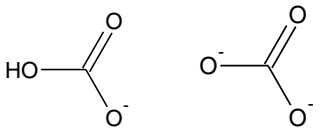 |

Besides the aqueous-phase chemical equilibrium reactions set up in the Independence model for PZ-$H_2O$-$CO_2$, the following reactions involving AEP species were used in this study.

$$AEP + H^+ \leftrightarrow AEPH^+$$

$$AEPH^+ + H^+ \leftrightarrow AEP(H^+)_2$$
$$AEPCOO^- + H^+ \leftrightarrow H^+AEPCOO^-$$
$$^-OOCAEP + H^+ \leftrightarrow {}^-OOCAEPH^+$$
$$H^+AEPCOO^- + H^+ \leftrightarrow (H^+)_2 AEPCOO^-$$
$$^-OOCAEPH^+ + H^+ \leftrightarrow (H^+)_2 AEPCOO^-$$
$$AEP(COO^-)_2 + H^+ \leftrightarrow H^+AEP(COO^-)_2$$
$$AEP + HCO_3^- \leftrightarrow AEPCOO^- + H_2O$$
$$AEP + HCO_3^- \leftrightarrow {}^-OOCAEP + H_2O$$
$$AEPH^+ + HCO_3^- \leftrightarrow H^+AEPCOO^- + H_2O$$
$$AEPCOO^- + HCO_3^- \leftrightarrow AEP(COO^-)_2 + H_2O$$
$$^-OOCAEP + HCO_3^- \leftrightarrow AEP(COO^-)_2 + H_2O$$
$$H^+AEPCOO^- + HCO_3^- \leftrightarrow H^+AEP(COO^-)_2 + H_2O$$
$$^-OOCAEPH^+ + HCO_3^- \leftrightarrow H^+AEP(COO^-)_2 + H_2O$$

AEP is an existing component in the Aspen Plus® databank. Other AEP-related species were added as new components. Following the treatment in the Independence model, AEP and zwitterions ($H^+AEPCOO^-$ and $^-OOCAEPH^+$) were modeled as Henry's components. Zwitterions were assigned an extremely low Henry's constant as they are expected to be non-volatile.

*2.1.1. Reference state and units*

In the Independence model, two different reference states are used depending on whether the species in consideration is a solvent or solute and the same treatment is followed in this work. The symmetric convention is applied for water as a solvent with the reference state as pure solvent at the system temperature and pressure:

$$\gamma_s \to 1 \text{ as } x_s \to 1 \tag{1}$$

The asymmetric convention was used for solutes (AEP, zwitterion, and ions) with the reference state as infinite dilution in water at the temperature and pressure of the system:

$$\gamma_i^* \to 1 \text{ as } x_i \to 0 \tag{2}$$

where $\gamma_s$ is the symmetric activity coefficient of solvent and $\gamma_i$* the asymmetric activity coefficient of solutes.

*2.1.2. Reaction equilibrium*

The reaction equilibrium constant is expressed as follows:

$$K_j = \prod_i a_i^{v_{ij}} = \prod_i (x_i \gamma_i)^{v_{ij}} \tag{3}$$

where $K_j$ is the equilibrium constant of reaction $j$ on a mole fraction scale; $a_i$ is the activity of component $i$; $v_{ij}$ is the stoichiometric coefficient of component $i$ in reaction $j$; $x_i$ and $\gamma_i$ are the mole fraction and the activity coefficient of component $i$, respectively. The chemical equilibrium constant was determined from the Gibbs free energy change of the reaction.

$$-\ln K_j = \frac{\Delta G_j(T)}{RT} \tag{4}$$

where $\Delta G_j(T)$ is the Gibbs free energy change for reaction $j$ at system temperature; $\Delta G_j(T)$ is defined as the difference between the Gibbs free energy of formation of the products and reactants at their reference state, $G_i(T)$, weighted by their stoichiometric coefficients.

$$\Delta G_j(T) = \sum_i v_{ij} G_i(T) \tag{5}$$

For solvents (water in this work), the Gibbs free energy of formation in their reference state (pure solvent) was calculated from that of ideal gas and the departure function:

$$G_s(T) = G_s^{ig}(T) + \Delta G_s^{ig \to l}(T) \tag{6}$$

The ideal gas Gibbs free energy of formation of the solvent was calculated from the following equation:

$$G_s^{ig}(T) = \Delta_f H_{s,298.15}^{ig} + \int_{298.15}^{T} C_{P,s}^{ig} dT - T \times \left( \frac{\Delta_f H_{s,298.15}^{ig} - \Delta_f G_{s,298.15}^{ig}}{298.15} + \int_{298.15}^{T} \frac{C_{P,s}^{ig}}{T} dT \right) \tag{7}$$

where $\Delta_f H_{s,298.15}^{ig}$ and $\Delta_f G_{s,298.15}^{ig}$ are ideal gas enthalpy of formation and ideal gas Gibbs free energy of formation of solvent s at 298.15 K, respectively, and $C_{P,s}^{ig}$ the ideal gas heat capacity of solvent *s*. The standard state thermodynamic properties of water ($\Delta_f H_{s,298.15}^{ig}$, $C_{P,s}^{ig}$, and $\Delta_f G_{s,298.15}^{ig}$) exist in the Aspen Plus® databank. The Gibbs free energy departure function for water was obtained from the ASME steam table. For molecular solutes ($CO_2$, AEP, and $H^+AEPCOO^-$), the Gibbs free energy in their reference state (infinite dilution in aqueous phase), $G_i^{\infty,aq}(T)$, was calculated from Henry's law:

$$G_i^{\infty,aq}(T) = G_i^{ig}(T) + RT \ln\left( \frac{H_{i,s}(T,P)}{P^{ref}} \right) \tag{8}$$

where $H_{i,s}(T,P)$ is the Henry's constant of molecular solute *i* in solvent *s* at system temperature T and pressure P; $P^{ref}$ the reference pressure of 1 bar, and $G_i^{ig}(T)$ the ideal gas Gibbs free energy of formation of molecular solute *i*, which is calculated in the same way as for the solvent:

$$G_i^{ig}(T) = \Delta_f H_{i,298.15}^{ig} + \int_{298.15}^{T} C_{P,i}^{ig} dT - T \times \left( \frac{\Delta_f H_{i,298.15}^{ig} - \Delta_f G_{i,298.15}^{ig}}{298.15} + \int_{298.15}^{T} \frac{C_{P,i}^{ig}}{T} dT \right) \tag{9}$$

where $\Delta_f H_{i,298.15}^{ig}$ and $\Delta_f G_{i,298.15}^{ig}$ are ideal gas enthalpy of formation and ideal gas Gibbs free energy of formation of molecular solute *i* at 298.15 K, respectively, and $C_{P,i}^{ig}$ is the ideal gas heat capacity of molecular solute *i*.

$\Delta_f H_{i,298.15}^{ig}$, $\Delta_f G_{i,298.15}^{ig}$, and $C_{P,i}^{ig}$ of $CO_2$ and AEP exist in the Aspen Plus® databank. The difference of $\Delta_f H_{i,298.15}^{ig}$ and $\Delta_f G_{i,298.15}^{ig}$ between $H^+AEPCOO^-$/$^-OOCAEPH^+$ and the parent amine, AEP, were assumed to be the same as the difference between $H^+PZCOO^-$ and PZ in the Independence model. These estimated values were used as initial guess in the regression of the data of $CO_2$ solubility in aqueous AEP solution, from which the final values of these parameters of $H^+AEPCOO^-$ and $^-OOCAEPH^+$ were obtained. $C_{P,i}^{ig}$ of $H^+AEPCOO^-$ and $^-OOCAEPH^+$ were estimated based on the ratio of their molecular weight to AEP. $C_{P,i}^{ig}$ of AEP, $H^+AEPCOO^-$, and $^-OOCAEPH^+$ were fixed in future regressions.

The Henry's constant, $H_{i,s}(T,P)$, was calculated from

$$H_{i,s}(T,P) = H_{i,s}(T,P_s^{*,l}) \exp\left(\frac{1}{RT}\int_{P_s^{*,l}}^{P} V_{i,s}^{\infty} dP\right) \tag{10}$$

where $H_{i,s}(T,P_s^{*,l})$ is the Henry's constant of molecular solute *i* in solvent *s* at system temperature T and the solvent vapor pressure; $P_s^{*,l}$ (obtained from the Antoine model), and $V_{i,s}^{\infty}$ the partial molar volume of molecular solute *i* at infinite dilution in solvent *s* at T and P (calculated from the Brelvi-O'Connell model [11] by using their critical properties). The Poynting pressure correction factor (the exponent term) accounts for the effect of pressure on Henry's constant, and is almost unity and can be ignored at low pressures. $H_{i,s}(T,P_s^{*,l})$ was calculated using the following correlation in Aspen Plus®:

$$\ln H_{i,s} = a_{i,s} + \frac{b_{i,s}}{T} + c_{i,s} \times \ln(T) + d_{i,s} \times T \tag{11}$$

The Henry's coefficients, $a_{i,s}$, $b_{i,s}$, $c_{i,s}$, $d_{i,s}$ of $CO_2$ in water are available in the Aspen Plus® databank, while the Henry's coefficients of AEP in water were obtained from regression of aqueous AEP volatility data.

For ionic solutes, the Gibbs free energy of formation in their reference state (infinite dilution in aqueous phase) at system temperature, $G_i^{\infty,aq}(T)$, were calculated from the enthalpy of formation and Gibbs free energy of formation in aqueous-phase infinite dilution at 298.15 K, and the heat capacity in aqueous-phase infinite dilution.

$$G_i^{\infty,aq}(T) = \Delta_f H_{i,298.15}^{\infty,aq} + \int_{298.15}^{T} C_{P,i}^{\infty,aq} dT - T \times \left(\frac{\Delta_f H_{i,298.15}^{\infty,aq} - \Delta_f G_{i,298.15}^{\infty,aq}}{298.15} + \int_{298.15}^{T} \frac{C_{P,i}^{\infty,aq}}{T} dT\right) + RT \ln\left(\frac{1000}{M_w}\right) \tag{12}$$

The term $RT\ln(1000/M_w)$ is added because $\Delta_f G_{i,298.15}^{\infty,aq}$, as reported in the literature, is based on molality scale, while $G_i^{\infty,aq}(T)$ is based on mole fraction scale. The standard state thermodynamic properties, $\Delta_f H_{i,298.15}^{\infty,aq}$, $\Delta_f G_{i,298.15}^{\infty,aq}$, and $C_{P,i}^{\infty,aq}$, for AEP-related ionic species are not available in the Aspen Plus® databank. The $\Delta_f H_{i,298.15}^{\infty,aq}$ and $\Delta_f G_{i,298.15}^{\infty,aq}$ of $AEPH^+$ and $AEP(H^+)_2$ were calculated from the protonation reactions of $AEPH^+$ and $AEP(H^+)_2$ measured by Pagano [10].

$$\Delta_f G_{AEPH^+,298.15}^{\infty,aq} = \Delta_f G_{AEP,298.15}^{\infty,aq} + \Delta_r G_i = \Delta_f G_{AEP,298.15}^{\infty,aq} - RT\ln K_{m,i} \tag{13}$$

$$\Delta_f H_{AEPH^+,298.15}^{\infty,aq} = \Delta_f H_{AEP,298.15}^{\infty,aq} + \Delta_r H_i \tag{14}$$

$$\Delta_f G_{AEP(H^+)_2,298.15}^{\infty,aq} = \Delta_f G_{AEPH^+,198.15}^{\infty,aq} + \Delta_r G_i = \Delta_f G_{AEP,298.15}^{\infty,aq} - RT\ln K_{m,i} \tag{15}$$

$$\Delta_f H_{AEP(H^+)_2,298.15}^{\infty,aq} = \Delta_f H_{AEPH^+,298.15}^{\infty,aq} + \Delta_r H_i \tag{16}$$

where $\Delta_r G_i$ , $\Delta_r H_i$ , and $K_{m,i}$ are Gibbs free energy change, enthalpy change, and molality scale protonation constants of a certain reaction; $\Delta_f G^{\infty,aq}_{AEP,298.15}$ and $\Delta_f H^{\infty,aq}_{AEP,298.15}$ are Gibbs free energy of formation and enthalpy of formation of AEP in aqueous-phase infinite dilution at 298.15 K, which can be obtained from Henry's law as follows:

$$\Delta_f G^{\infty,aq}_{AEP,298.15} = \Delta_f G^{ig}_{AEP,298.15} + R \times 298.15 \times \ln\left(\frac{H_{AEP,s,298.15}}{P^{ref}}\right) - RT\ln\left(\frac{1000}{M_w}\right) \tag{17}$$

$$\Delta_f H^{\infty,aq}_{AEP,298.15} = \Delta_f H^{ig}_{AEP,298.15} + R\,\frac{\partial \ln H_{AEP,H_2O}}{\partial\,(1/T)} \tag{18}$$

The term $RT\ln(1000/M_w)$ is subtracted because $\Delta_f G^{\infty,aq}_{i,298.15}$ in Aspen Plus® is based on molality scale, while $\Delta_f G^{ig}_{i,298.15}$ (as provided in the databank) is based on mole fraction scale. The conversion of equilibrium constants from molality scale to mole fraction scale can be found in Hilliard [8]. $\Delta_f G^{\infty,aq}_{i,298.15}$ and $\Delta_f H^{\infty,aq}_{i,298.15}$ of other AEP-related ions were initially estimated based on the assumption that the difference between AEP-related species is the same as the difference between corresponding PZ-related species. For example, we assume:

$$\Delta_f H^{\infty,aq}_{AEPCOO^-,298.15} - \Delta_f H^{\infty,aq}_{AEP,298.15} = \Delta_f H^{\infty,aq}_{PZCOO^-,298.15} - \Delta_f H^{\infty,aq}_{PZ,298.15}$$

and

$$\Delta_f H^{\infty,aq}_{AEP(COO^-)_2,298.15} - \Delta_f H^{\infty,aq}_{AEPCOO^-,298.15} = \Delta_f H^{\infty,aq}_{PZ(COO^-)_2,298.15} - \Delta_f H^{\infty,aq}_{PZCOO^-,298.15}$$

These values were used as an initial guess in the regression of the $CO_2$ solubility in aqueous AEP solution, from which the final value of these parameters was obtained. $C^{\infty,aq}_{P,i}$ of AEP was assumed to be the same as $C^{ig}_{P,i}$ of AEP, and then $C^{\infty,aq}_{P,i}$ of other AEP species was estimated based on the ratio of their molecular weight to AEP. $C^{\infty,aq}_{P,i}$ of all AEP species was fixed in future regressions.

### *2.2. Vapor-liquid phase equilibrium*

Phase equilibrium governs the distribution of molecular species between the vapor and liquid phase. In the activity coefficient approach, the basic vapor-liquid equilibrium relationship for solvent is represented by:

$$\varphi^V_s y_s P = \gamma_s x_s P^{*,l}_s \exp\left(\frac{1}{RT}\int_{P^{*,l}_s}^{P} V^{*,l}_s dP\right) \tag{19}$$

where $\varphi^V_s$ is the vapor phase fugacity coefficient of solvent s, $\gamma_s$ the symmetric activity coefficient of solvent *s*, $P^{*,l}_s$ the solvent vapor pressure at system temperature, and $V^{*,l}_s$ the liquid pure component molar volume of solvent *s* calculated from the Rackett model. For molecular solutes, Henry's Law was used to determine vapor-liquid equilibrium:

$$\varphi^V_i y_i P = \gamma^*_i x_i H_{i,s}(T, P^{*,l}_s) \exp\left(\frac{1}{RT}\int_{P^{*,l}_s}^{P} V^{\infty}_{i,s} dP\right) \tag{20}$$

where $\gamma^*_i$ is the symmetric activity coefficient of component *i*.

*2.3. Vapor phase behavior*

Vapor phase behavior was modeled using the Redlich-Kwong-Soave (RKS) equation of state:

$$P = \frac{RT}{V-b} - \frac{a}{V(V-b)} \tag{21}$$

T and P represent the temperature and pressure of the vapor phase and R represents the gas constant. The attraction between molecules and their size are represented in the equation by parameters a and b respectively, which are calculated from critical properties.

*2.4. System non-idealities*

Vapor phase non-idealities (fugacity) are calculated using the SRK equation of state. Liquid phase non-idealities (activity) are calculated using the eNRTL model [6]. The use of the eNRTL model in amine/acid gas systems has been described previously by Posey [7] and Frailie [9]. The basic postulate of this model is that the excess Gibbs energy of an aqueous electrolyte system can be written as the sum of three contributions: the NRTL term (related to the local ion-molecule, ion-ion, and molecule-molecule interactions that exist in the immediate neighborhood of any species), the PDH term (related to the long-range ion-ion interactions that exist beyond the immediate neighborhood of a central ionic species) and the Born term (accounts for the excess Gibbs energy of transfer from infinite dilution in the mixed solvent to infinite dilution in the aqueous phase).

$$g_i^{ex^*} = g_{PDH,i}^{ex^*} + g_{Born,i}^{ex} + g_{NRTL,i}^{ex^*} \tag{22}$$

Accordingly,

$$\ln \gamma_i = \ln \gamma_i^{PDH} + \ln \gamma_i^{Born} + \ln \gamma_i^{NRTL} \tag{23}$$

The adjustable parameters for the eNRTL model include the pure component dielectric constant coefficient, Born radius of ionic species, and NRTL parameters for molecule-molecule, molecule-electrolyte, and electrolyte-electrolyte pairs. The NRTL parameters are the nonrandomness factors and binary interaction parameters. Following the treatment for PZ in the Independence model, dielectric constants of AEP are assumed to be the same as MEA; ionic radii were assigned default values of 3 Å; the nonrandomness factor was fixed at 0.3 for molecule-molecule pairs and 0.2 for molecule-electrolyte and electrolyte-electrolyte pairs, and binary interaction parameters for electrolyte-electrolyte pairs were set to zero. Therefore, the only adjustable parameters of the eNRTL model in this work were binary interaction parameters for molecule-molecule pairs and for electrolyte-molecule pairs, as expressed in the following relationships as a function of temperature. Molecule-molecule binary interaction parameters:

$$\tau_{mm'} = A_{mm'} + \frac{B_{mm'}}{T} + C_{mm'} \ln(T) + D_{mm'} T \tag{24}$$

Electrolyte-molecule (or molecule-electrolyte) binary interaction parameters:

$$\tau_{x,y} = E_{x,y} + \frac{F_{x,y}}{T} \tag{25}$$

$$\tau_{x,y} = \tau_{ca,m} \text{ or } \tau_{m,ca} \tag{26}$$

Subscripts and indices of *m*, *c*, and *a* refer to molecules, cations, and anions, respectively. $\tau_{mm'}$, $\tau_{ca,m}$, and $\tau_{m,ca}$ can be obtained from the regression of amine volatility data and $CO_2$ solubility data.

The parameters used in this model are summarized in Table 2. All model parameters not mentioned in Table 1 were either from the Independence model or set to Aspen Plus® default values.

Table 2. Summary of model parameters

| Parameters | Component | Source | Data for regression |
|---|---|---|---|
| $\Delta_f G^{ig}_{s,298.15}$ | AEP | Aspen Plus® Databank | —— |
| | $H^+AEPCOO^-$ / $^-OOCAEPH^+$ | Regression | VLE and NMR for AEP-$H_2O$-$CO_2$ |
| $\Delta_f H^{ig}_{s,298.15}$ | AEP | Aspen Plus® Databank | —— |
| | $H^+AEPCOO^-$/ $^-OOCAEPH^+$ | Regression | VLE and NMR for AEP-$H_2O$-$CO_2$ |
| $C^{ig}_{P,s}$ | AEP | Aspen Plus® Databank | —— |
| | $H^+AEPCOO^-$/ $^-OOCAEPH^+$ | Ratio to $C^{ig}_{P,s}$ of AEP | —— |
| $\Delta_f G^{\infty,aq}_{i,298.15}$ | $AEPH^+$/$AEP(H^+)_2$ | Pagano [10] | —— |
| | Other AEP ions | Regression | VLE and NMR for AEP-$H_2O$-$CO_2$ |
| $\Delta_f H^{\infty,aq}_{i,298.15}$ | $AEPH^+$/$AEP(H^+)_2$ | Pagano [10] | —— |
| | Other AEP ions | Regression | VLE and NMR for AEP-$H_2O$-$CO_2$ |
| $C^{\infty,aq}_{P,i}$ | All AEP species | Ratio to $C^{ig}_{P,s}$ of AEP | —— |
| Henry's constant | AEP/$H_2O$ | Regression | Volatility of AEP |
| | $H^+AEPCOO^-$ / $H_2O$ | Assumed same as $H^+PZCOO^-$/ $H_2O$ | —— |
| | $^-OOCAEPH^+$ / $H_2O$ | | |
| Dielectric constant | AEP | Assumed same as PZ | —— |
| NRTL binary interaction parameters | AEP/$H_2O$ | Regression | Volatility of AEP |
| | AEP cation, PZ anion/ $H_2O$<br>PZ cation, AEP anion/ $H_2O$<br>AEP cation, AEP anion/ $H^+PZCOO^-$<br>PZ cation, PZ anion/ $H^+AEPCOO^-$<br>PZ cation, PZ anion/ $^-OOCAEPH^+$ | Regression | VLE for PZ-AEP- $H_2O$-$CO_2$ |

## 3. Results and Discussion

### *3.1. Identification of $^{13}C$ NMR spectra*

Quantitative $^{13}C$ NMR was used in this work to investigate the species distribution in AEP-$H_2O$-$CO_2$ and PZ-AEP-$H_2O$-$CO_2$, and validate the model prediction of speciation. Due to the rapid exchange rate of protons, a protonated/di-protonated species and the unprotonated counterparts cannot be differentiated by the NMR spectroscopy used in this study. Therefore the sum of these was quantified from the NMR spectra. Potential species in the PZ-AEP-$H_2O$-$CO_2$ system are listed in Table 1. The identification of NMR peaks in loaded 6 m AEP and 5 m PZ/2 m AEP is shown in Figure 1. Due to the long distance between the primary and secondary amino groups in AEP, the addition of a carboxyl group to a $-NH_2$ does not affect the chemical shift of the C on the other side. This led to the overlap of peaks from different species as shown in Figure 1.

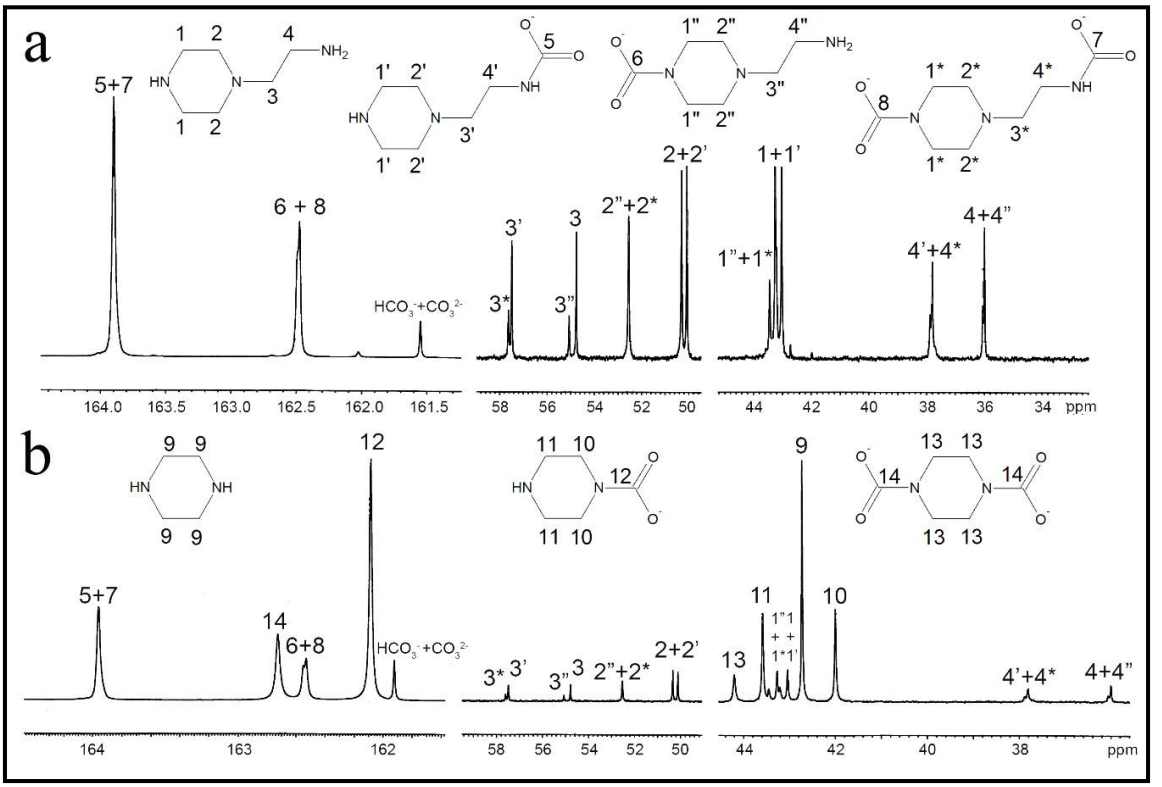


Fig. 1. $^{13}C$ NMR spectra for 6 m AEP (a) and 5 m PZ/2 m AEP (b) at 25 °C and $CO_2$ loading of 0.3

### *3.2. AEP-$H_2O$*

The amine vapor pressure of 0.7 m and 5 m AEP from 40–70 °C has been measured in a stirred reactor coupled with a hot gas FTIR analyzer (Fourier Transform Infrared Spectroscopy, Temet Gasmet Dx-4000). The details of the experimental apparatus, procedure, and analytical methods were described by Nguyen [12]. The volatility data were regressed to determine Henry's constant coefficients of AEP in water (Equation 11) and molecule-molecule binary interaction parameters $\tau_{mm'}$ for the AEP/$H_2O$ pair (Equation 24). The regression results are given in Table 3. All parameters concerning AEP/$H_2O$ were held constant during subsequent regressions. After the regression, the model predicts the volatility of AEP well (Figure 2). The volatility of AEP was found to be just 1% of the volatility of aqueous PZ with similar alkalinity and no $CO_2$ loading, indicating a negligible amine loss owing to volatilization, but a potential difficulty with thermal reclaiming.

Table 3. Regressed parameters and standard error for AEP/$H_2O$ regression

| Parameter | Species | Value (SI units) | Standard deviation |
|---|---|---|---|
| $\tau_{mm'}$/1 | $H_2O$/AEP | 3.3 | 0.19 |
| Henry/1 | AEP/$H_2O$ | 36 | 1.5 |
| Henry/2 | AEP/$H_2O$ | -10780 | 507 |

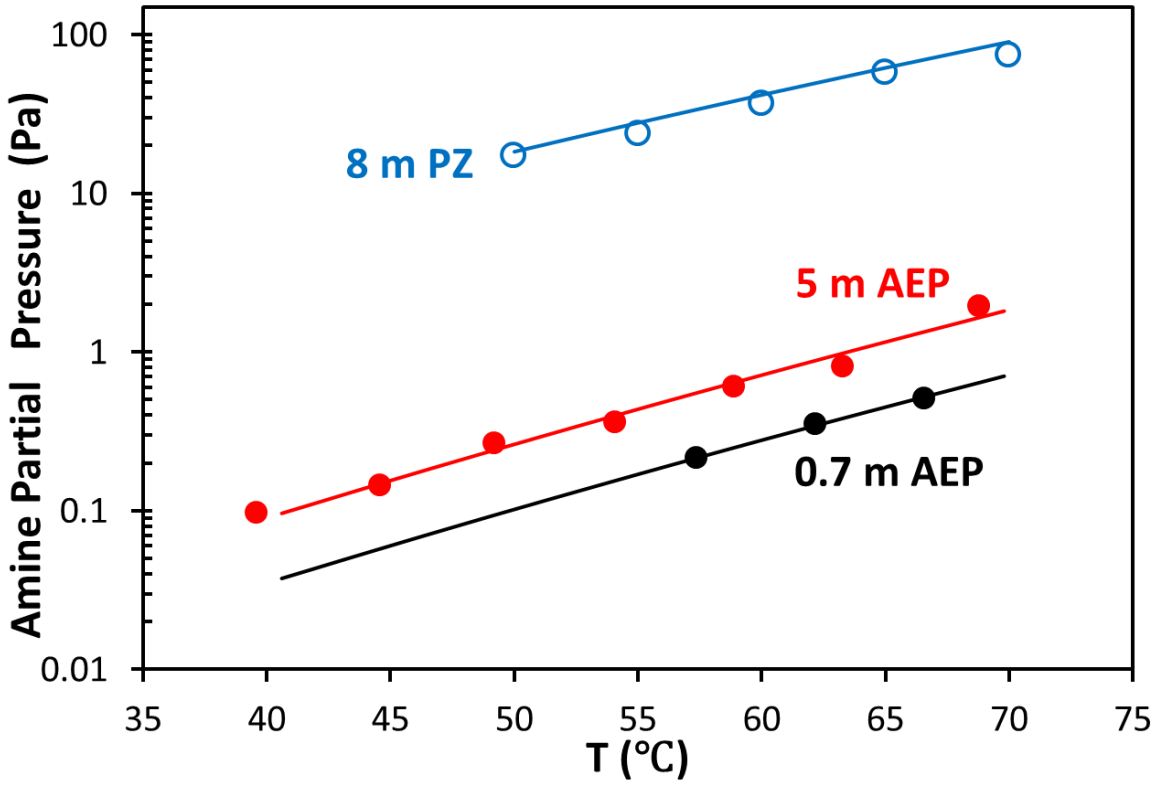


Fig. 2. AEP vapor pressure predicted by the model compared with experimental data, as well as data for 8 m PZ with no $CO_2$ loading [12]. Filled points: Experimental data; Solid lines: Model prediction from this work.

### *3.3. AEP-$H_2O$-$CO_2$*

The vapor-liquid equilibrium (VLE) of $CO_2$ for 6 m AEP has been measured with a wetted wall column at temperatures up to 100 °C [12]. These $CO_2$ solubility data were used for data regression. After the initial regression of the VLE data the model did not predict the speciation. As Aspen Plus® is not configured to regress speciation data, the free energy of formation of AEP carbamate species was manually adjusted to fit the NMR speciation data at 25 °C, and then standard enthalpies of formation were regressed again to get a better prediction of $CO_2$ solubility. This process was repeated to get a reasonable prediction for both $CO_2$ solubility and speciation (Figures 3 and 4). From the VLE prediction, the $CO_2$ cyclic capacity of this solvent is calculated as 0.71 mol/kg (AEP + water), using the following equation.

$$Capacity = \frac{(\alpha_{rich} - \alpha_{lean}) * mol\ \text{alkalinity}}{kg(\text{amine}+H_2O)} = \frac{mol\ CO_2}{kg} \quad (27)$$

where $\propto_{lean}$ and $\propto_{rich}$ are defined as the $CO_2$ loading with $P_{CO2*}$ of 0.5 and 5 kPa at 40 °C. The determined parameters are given in Table 4.

As noted previously, the original species and their protonated/di-protonated species cannot be differentiated in the NMR spectra, so they were quantified as a group in Figure 4. At $CO_2$ loading below 0.2 mol $CO_2$/mol alkalinity, $AEPCOO^-/H^+AEPCOO^-$ is the dominant $CO_2$ sink, followed by $^-OOCAEP/^-OOCAEPH^+$. At $CO_2$ loading above 0.25 mol $CO_2$/mol alkalinity, the fraction of $CO_2$ in the form of monocarbamate decreases with $CO_2$ loading, due to its conversion to AEP dicarbamate and $HCO_3^-/CO_3^{2-}$. The fraction of AEP dicarbamate as a $CO_2$ sink increases with $CO_2$

loading and becomes dominant at $CO_2$ loading above 0.37 mol $CO_2$/mol alkalinity. Although the fraction of $HCO_3^-$ /$CO_3^{2-}$ as a $CO_2$ sink keeps increasing with loading, it is not a dominant one at loading below 0.4 mol $CO_2$/mol alkalinity.

Figure 5 shows the detailed predicted speciation for 6 m AEP at 40 °C. Free AEP decreases rapidly with $CO_2$ loading and is almost completely depleted at α = 0.3 mol/mol alkalinity. $AEPH^+$, $AEPCOO^-$, and $^-OOCAEP$ are the three major products in the lean loading range. As $CO_2$ loading increases to α = 0.35, the amount of $AEP(H^+)_2$, $H^+AEPCOO^-$, $^-OOCAEPH^+$, and $AEP(COO^-)_2$ is more and more significant. At α above 0.35, $AEP(H^+)_2$ and $H^+AEP(COO^-)_2$ are the two dominant species, followed by $HCO_3^-$. $(H^+)_2AEPCOO^-$, $CO_3^{2-}$, and free $CO_2$ are not significant species in the solution across the entire $CO_2$ loading range.

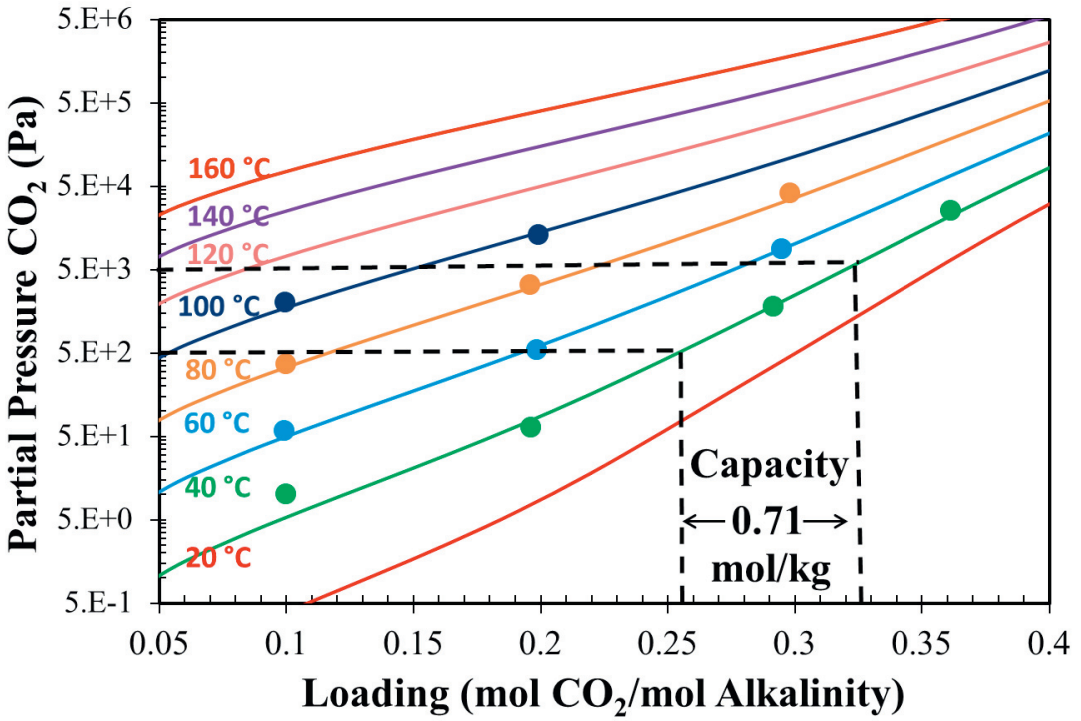


Fig. 3. Experimental measurement (points) [13] and Aspen Plus® predictions (lines) for VLE of loaded 6 m AEP solution between 20 °C and 160 °C

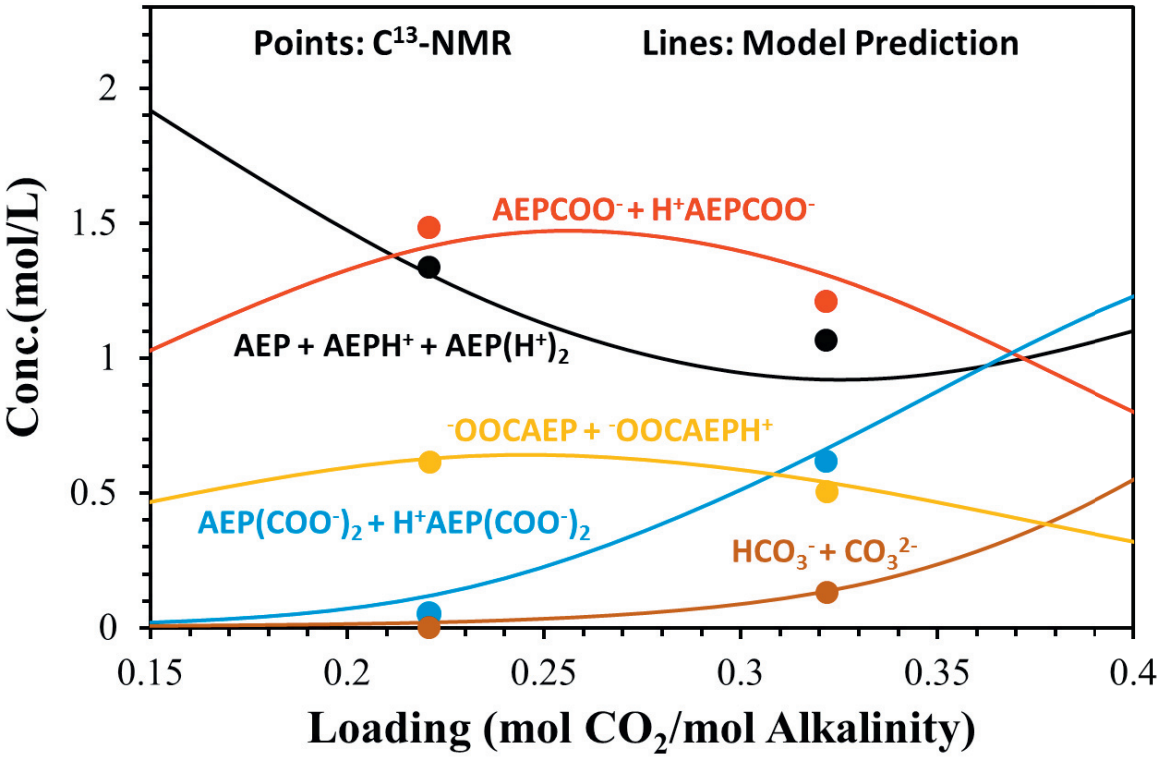


Fig. 4. $^{13}C$ speciation for 6 m AEP-$CO_2$-$H_2O$ at 25 °C

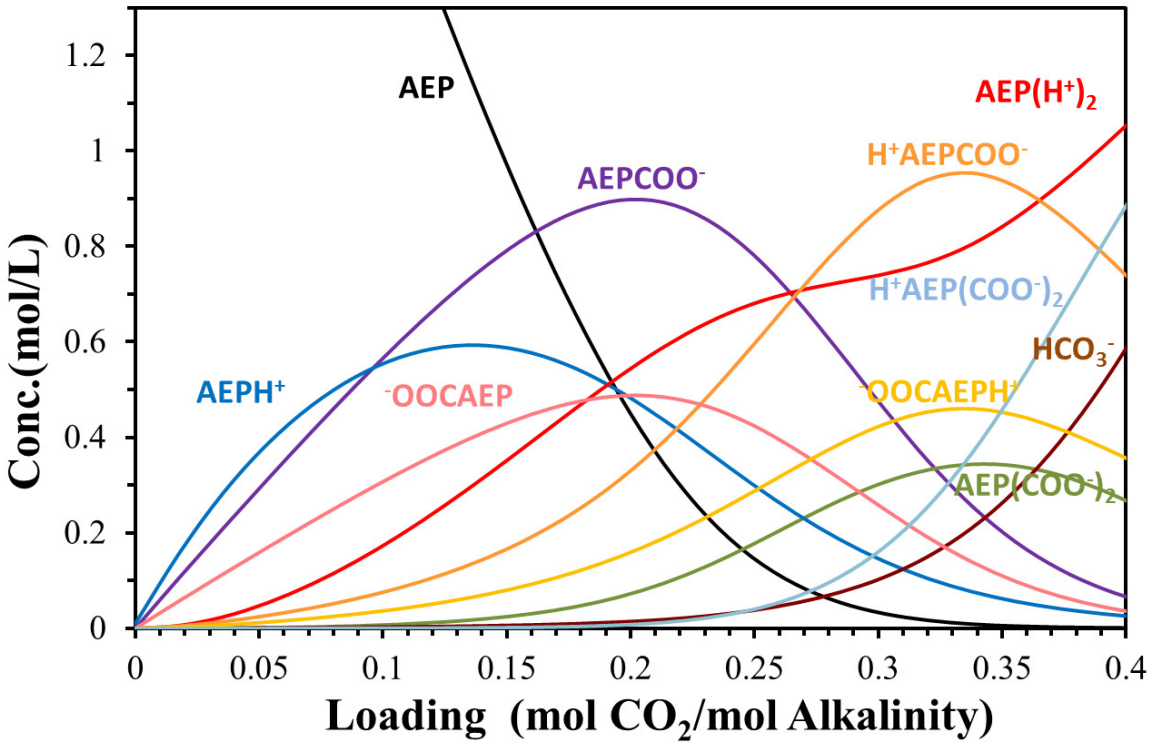


Fig. 5. Predicted speciation distribution for 6 m AEP-$CO_2$-$H_2O$ at 40 °C

Table 4. The adjusted parameters for 6 m AEP-$CO_2$-$H_2O$

| Parameter | Species | Value (kJ/mol) |
|---|---|---|
| $\Delta_f G^{\infty,aq}_{i,29815}$ | $AEPCOO^-$ | -99.9 |
| | $^-OOCAEP$ | -98.0 |
| | $H^+AEP(COO^-)_2$ | -501.5 |
| $\Delta_f G^{ig}_{s,29815}$ | $H^+AEPCOO^-$ | -93.5 |
| | $^-OOCAEPH^+$ | -91.2 |
| $\Delta_f H^{\infty,aq}_{i,298.15}$ | $AEPCOO^-$ | -523.9 |
| | $^-OOCAEP$ | -515.8 |
| | $H^+AEP(COO^-)_2$ | -963.4 |
| $\Delta_f H^{ig}_{s,29815}$ | $H^+AEPCOO^-$ | -550.5 |
| | $^-OOCAEPH^+$ | -540.1 |

*3.4. PZ/AEP/$H_2O$/$CO_2$*

The VLE of $CO_2$ for 5 m PZ/2 m AEP from 20–160 °C was regressed to determine NRTL binary interaction parameters for molecule-electrolyte pairs, $\tau_{ca,m}$, including AEP cation, PZ anion/$H_2O$ pairs; PZ cation, AEP anion/$H_2O$ pairs; AEP cation, AEP anion/$H^+PZCOO^-$ pairs; PZ cation, PZ anion/$H^+AEPCOO^-$ (Equation 25).

After regression, the VLE of $CO_2$ in 5 m PZ/2 m AEP is predicted well by the model (Figure 6), especially at the normal operating conditions of the absorber (40–60 °C and loading from 0.288–0.380). From the VLE prediction, the $CO_2$ cyclic capacity of this solvent is calculated as 0.86 mol/kg (PZ + AEP + water), compared to 0.50 mol/kg for 7 m MEA and 0.86 mol/kg for 8 m PZ. The higher $CO_2$ capacity leads to lower solvent flow rate for a specific $CO_2$ removal requirement, and thus less sensible heat demand for stripping. The regressed parameters are summarized in Table 5. The non-regressed or non-adjusted parameters used in this model are summarized in Table 6 (for non-temperature-dependence parameters) and Table 7 (for temperature-dependence parameters).

NMR measurement for 5 m PZ/2 m AEP at 25 °C was used to validate the prediction of speciation by this model. The prediction of the model is in good agreement with the experimental NMR measurements, except that the amount of AEP dicarbamate is underpredicted (Figure 7). $PZCOO^-/H^+PZCOO^-$ is the dominant $CO_2$ sink in the solution across the entire $CO_2$ loading range, followed by $AEPCOO^-/H^+AEPCOO^-$. The share of PZ dicarbamate as a $CO_2$ sink increases with $CO_2$ loading and becomes significant at rich $CO_2$ loading. The share of $OOCAEP/^-OOCAEPH^+$ and AEP dicarbamate as a $CO_2$ sink is not significant across the loading range, and the share of $HCO_3^-/CO_3^{2-}$ is negligible.

Figure 8 shows the detailed predicted speciation for 5 m PZ/2 m AEP at 40 °C. For simplicity, species with concentration below 0.1 mol/L across the entire loading range are not shown (including $AEPH^+$, $AEPCOO^-$, $^-OOCAEP$, $AEP(COO^-)_2$, $H^+AEP(COO^-)_2$, and $(H^+)_2AEPCOO^-$). Free PZ and AEP decreases drastically with $CO_2$ loading and are almost completely depleted at $\alpha$ = 0.35 mol/mol alkalinity. $PZH^+$ and $PZCOO^-$ are the two major products in the lean loading range and reach their maximum at $\alpha$ = 0.3 and $\alpha$ = 0.2 mol/mol alkalinity, respectively. As $CO_2$ loading increases, the amount of $H^+PZCOO^-$, $H^+AEPCOO^-$, $PZ(COO^-)_2$, and $AEP(H^+)_2$ is more and more significant. $HCO_3^-$ is not a significant species in the solution across the entire $CO_2$ loading range.

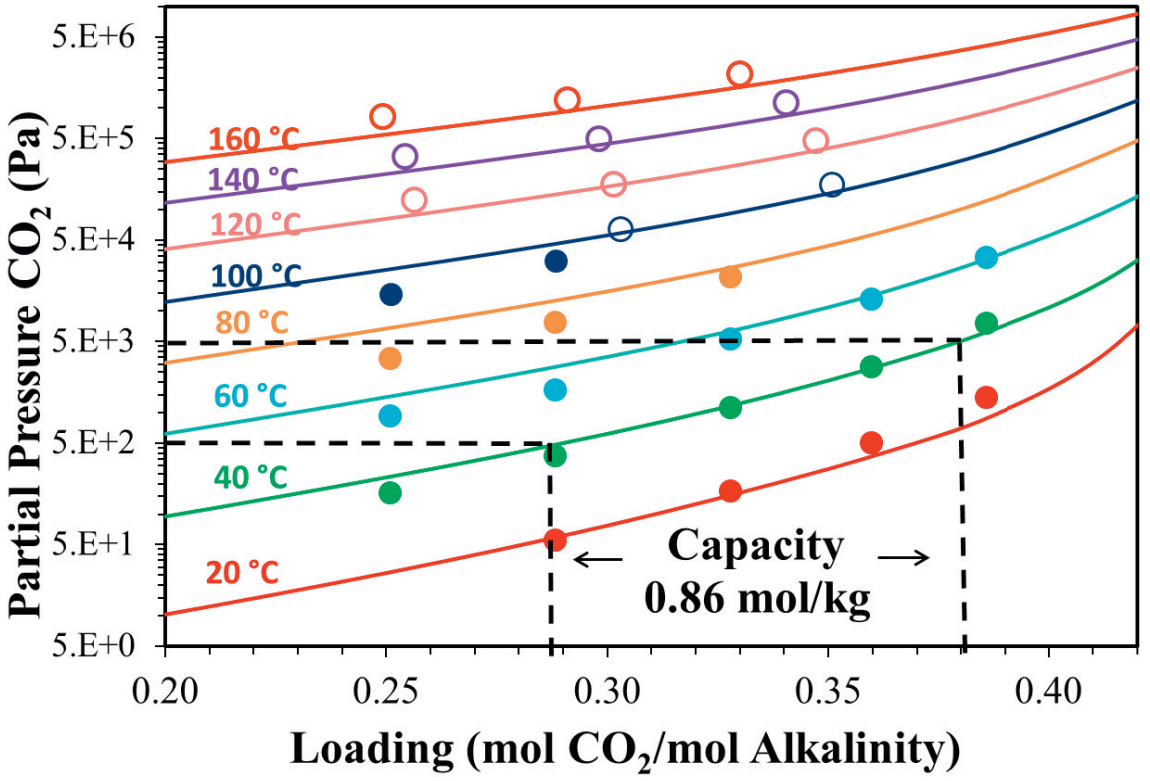

Fig. 6. Comparison of Aspen Plus® predictions (lines) and experimental data (points) for loaded 5 m PZ/2 m AEP between 20 °C and 160 °C

Table 5: Regressed parameters and standard error

| Parameter | Species | | Value | Standard error | Default |
|---|---|---|---|---|---|
| $\tau_{ca,m}$ | ($PZH^+$, $AEPCOO^-$) | $H_2O$ | -6.08 | 25 | -4 |
| | ($PZH^+$,$^-OOCAEP$) | $H_2O$ | -6.04 | 32 | -4 |
| | ($PZH^+$,$AEP(COO^-)_2$) | $H_2O$ | -5.20 | 39 | -4 |
| | ($AEP(H^+)_2$,$PZ(COO^-)_2$) | $H^+PZCOO^-$ | -7.01 | 9 | -2 |

Table 6: Summary of non-adjusted and non-temperature-dependence parameters used in this model

| Parameter | Species | Value (kJ/mol) |
|---|---|---|
| $\Delta_f G^{\infty,aq}_{i,298.15}$ | $AEPH^+$ | 210.4 |
| | $AEP(H^+)_2$ | 162.2 |
| | $(H^+)_2AEPCOO^-$ | -30.4 |
| $\Delta_f H^{\infty,aq}_{i,298.15}$ | $AEPH^+$ | -117.0 |
| | $AEP(H^+)_2$ | -160.0 |
| | $(H^+)_2AEPCOO^-$ | -601.1 |

Table 7: Summary of non-adjusted and temperature-dependence parameters used in this model

| Comp. | Parameters | | | |
|---|---|---|---|---|
| | a | b | c | d |
| | Henry's constants (bar): $\ln H_{i,s} = a_{i,s} + \frac{b_{i,s}}{T} + c_{i,s} \times \ln(T) + d_{i,s} \times T$ | | | |
| $H^+AEPCOO^-/H_2O$ | -20 | 0 | 0 | 0 |
| $^-OOCAEPH^+/H_2O$ | -20 | 0 | 0 | 0 |
| | Ideal gas heat capacity(J/kmol-K): $C^{ig}_{P,i} = a_i + b_i \times T + c_i \times T^2 + d_{i,s} \times T^3$ | | | |
| $H^+AEPCOO^-$ | -54909 | 1289 | -0.96 | 0.00029 |
| $^-OOCAEPH^+$ | -54909 | 1289 | -0.96 | 0.00029 |
| | Aqueous Infinite Dilution Heat Capacity(J/kmol-K): $C^{\infty,aq}_{P,i} = a_i + b_i \times T + c_i \times T^2 + d_{i,s} / T$ | | | |
| $AEPH^+$ | -40709 | 956 | -0.71 | 0.00021 |
| $AEP(H^+)_2$ | -40709 | 956 | -0.71 | 0.00021 |
| $AEPCOO^-$ | -54909 | 1289 | -0.96 | 0.00029 |
| $^-OOCAEP$ | -54909 | 1289 | -0.96 | 0.00029 |
| $AEP(COO^-)_2$ | -68794 | 1615 | -1.20 | 0.00036 |

| | | | | |
|---|---|---|---|---|
| $H^+AEP(COO^-)_2$ | -68794 | 1615 | -1.20 | 0.00036 |
| $(H^+)_2AEPCOO^-$ | -54909 | 1289 | -0.96 | 0.00029 |

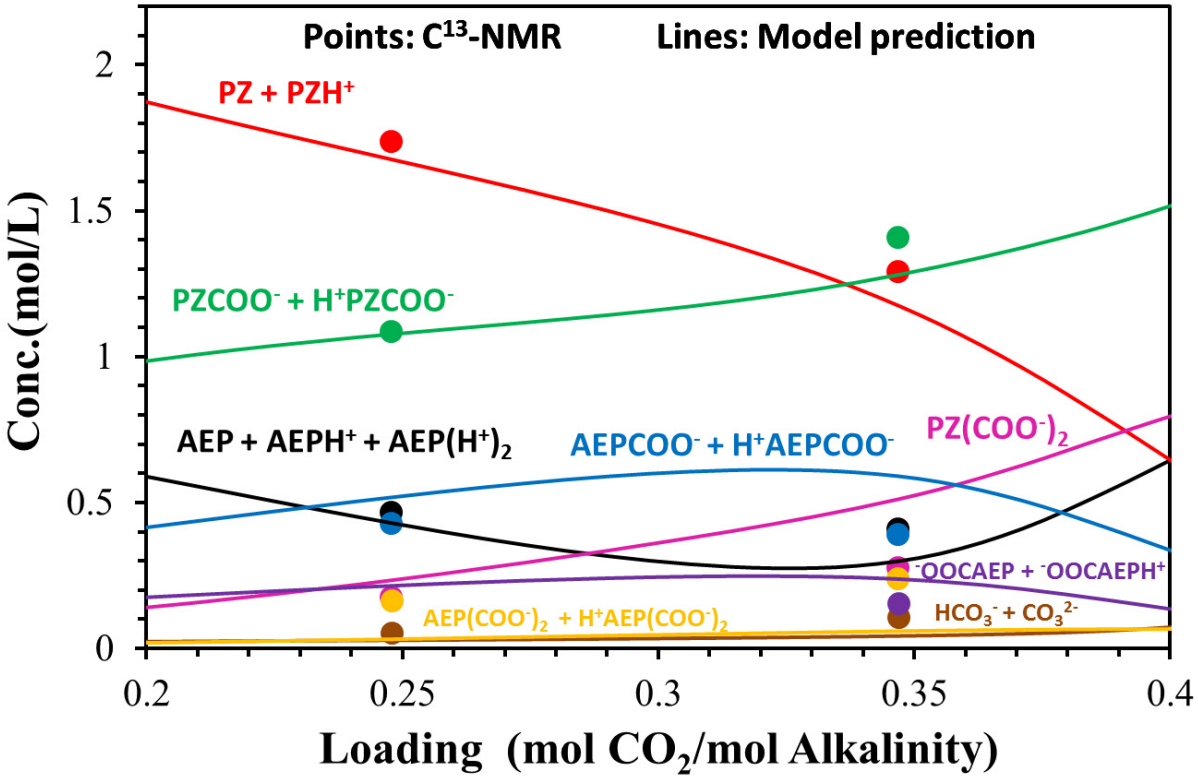


Fig. 7. Speciation validation for 5 m PZ/2 m AEP

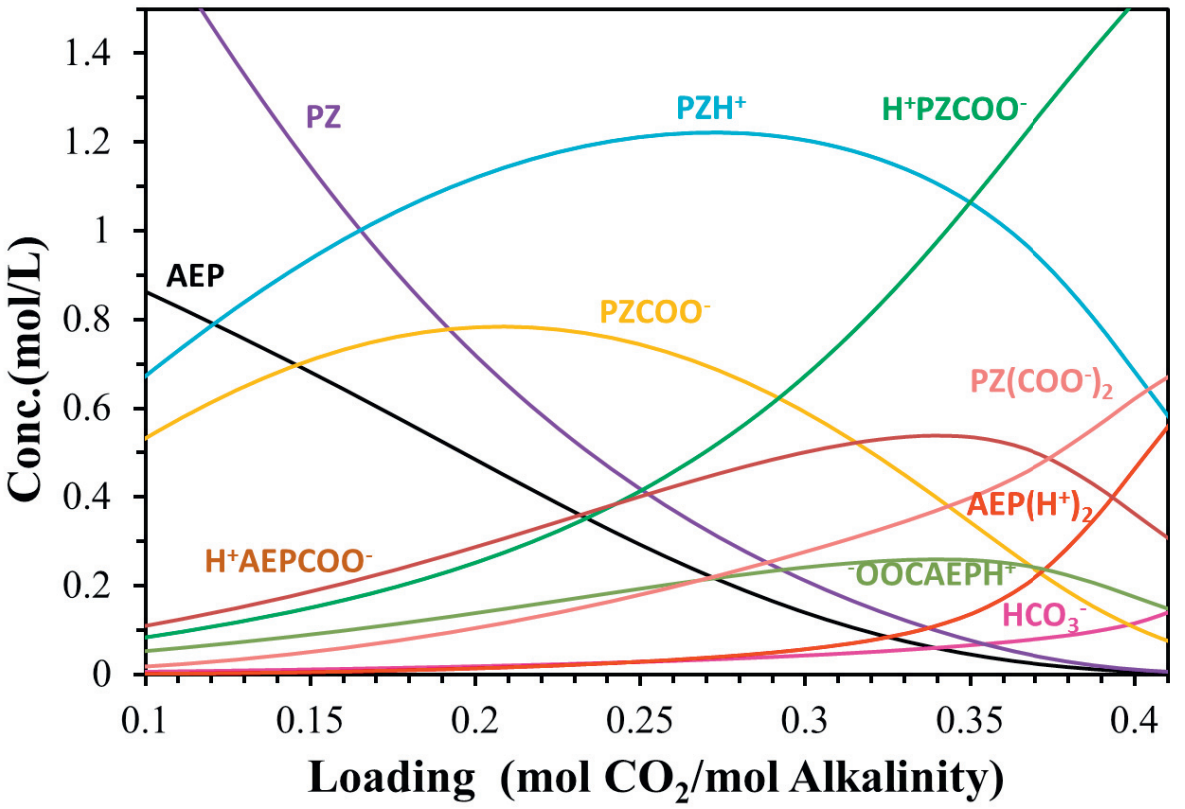


Fig. 8. Predicted speciation distribution for 6 m AEP-$CO_2$-$H_2O$ at 40 °C

### *3.5. Heat of absorption prediction*

The predicted heat of absorption for 6 m AEP and 5 m PZ/2 m AEP is shown in Figures 9 and 10. At 40 °C the heat of absorption of 6 m AEP is about 50–70 kJ/mol $CO_2$ in the operating loading range (0.255–0.325) and the heat of absorption of 5 m PZ/2 m AEP is around 75–85 kJ/mol $CO_2$ in the operating loading range (0.288–0.380). The decrease of heat of absorption with loading is due to the production of $HCO_3^-$ at rich loading, which gives a low enthalpy reaction between $CO_2$ and $H_2O$. Heat of absorption predictions in Aspen Plus® can be calculated using the calorimetric method and the Gibbs-Helmholtz equation. The use of these two methods to calculate heat of absorption has been described previously by Frailie [9]. In this model, these two methods give slightly inconsistent results of $H_{abs\text{-}CO2}$ at rich loading. The slight discrepancy of prediction is thought to be due to the inaccuracy of the calorimetric method.

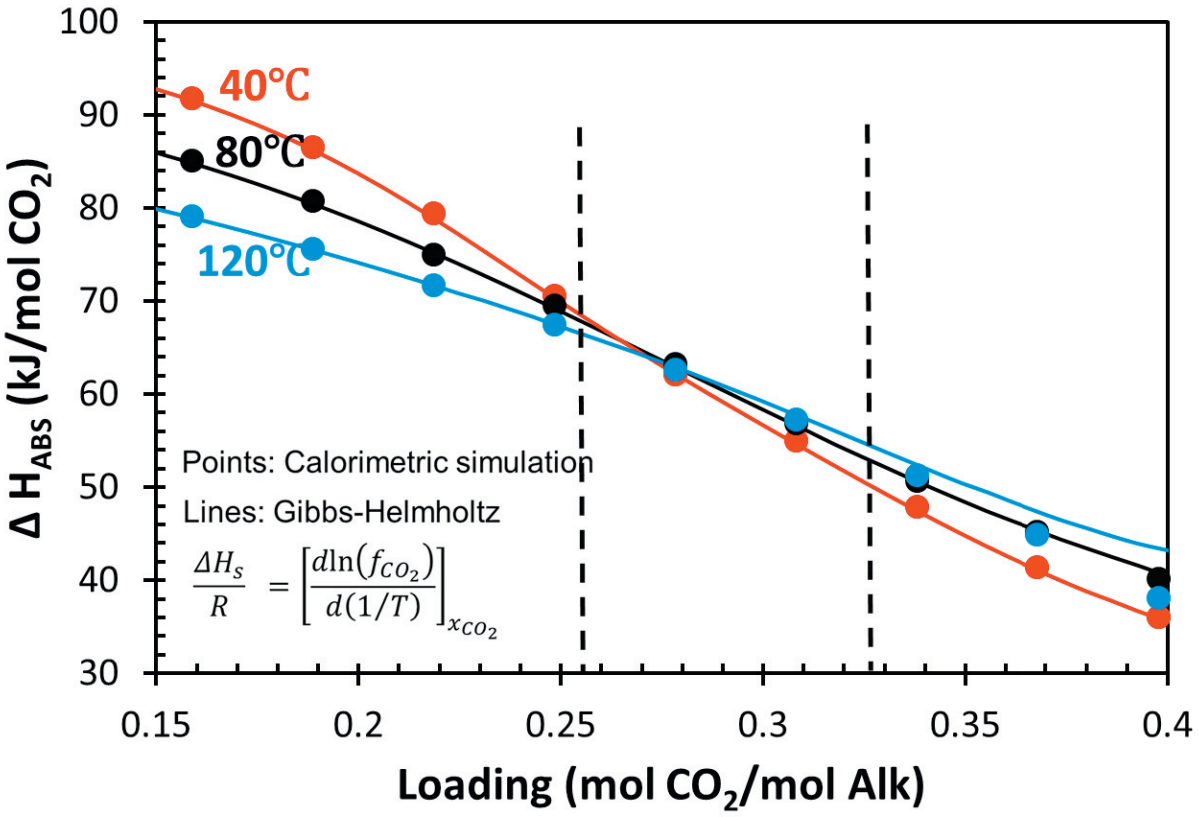


Fig. 9. Aspen Plus® model predictions of heat of absorption for 6 m AEP using Gibbs-Helmholtz (points) and calorimetric (lines) calculations

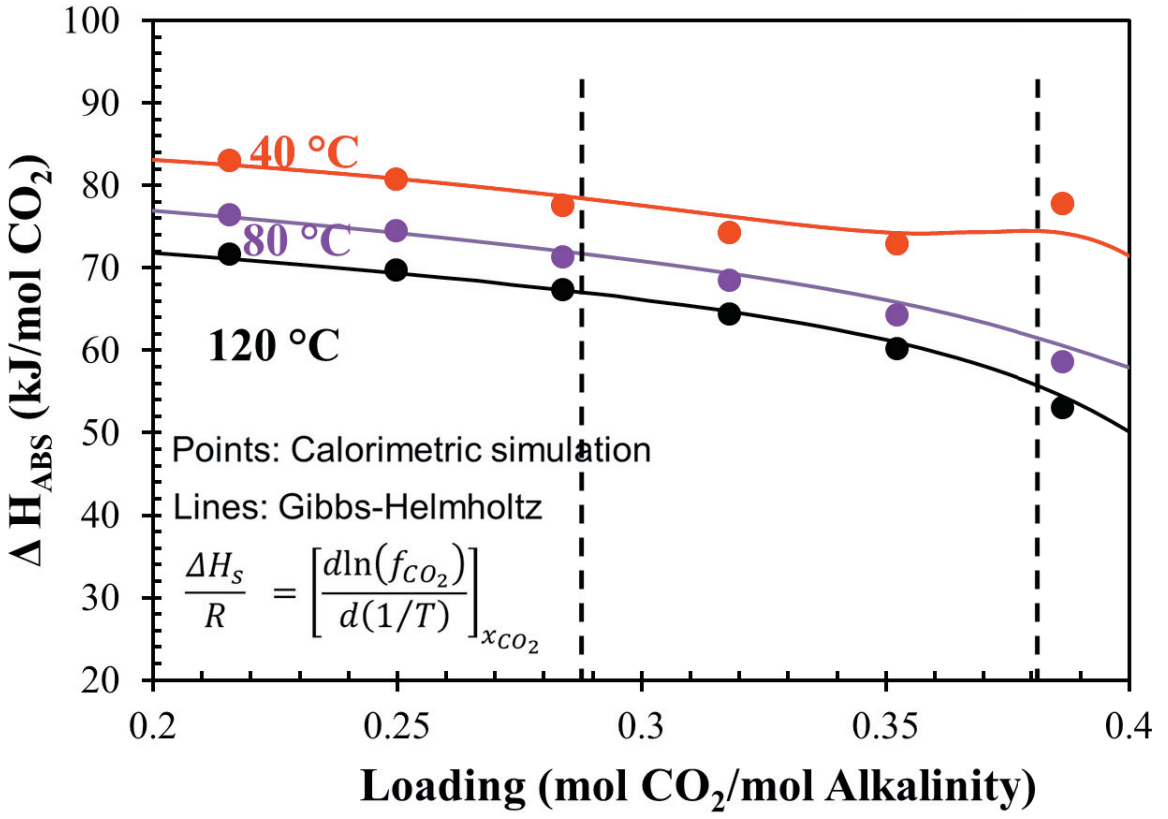


Fig. 10. Aspen Plus® model predictions of heat of absorption for 5 m PZ/2 m AEP using Gibbs-Helmholtz (points) and calorimetric (lines) calculations

**Conclusions**

A thermodynamic model was developed for PZ-AEP-$H_2O$-$CO_2$ in the framework of the eNRTL model by sequential data regression. The prediction for $CO_2$ solubility and speciation is in good agreement with the experimental data. From the VLE prediction, the $CO_2$ cyclic capacity of 6 m AEP is 0.71 mol/kg (AEP + water) and the $CO_2$ cyclic capacity of 5 m PZ/2 m AEP is 0.86 mol/kg (PZ + AEP + water).

Speciation prediction from the model shows that in AEP-H2O-CO2, at lean loading, AEPCOO-/H+AEPCOO- is the dominant $CO_2$ sink, followed by $^{-}$OOCAEP/$^{-}$OOCAEPH$^{+}$. The share of AEP dicarbamate as a $CO_2$ sink increases with $CO_2$ loading and becomes dominant at rich $CO_2$ loading. The share of $HCO_3^{-}$/$CO_3^{2-}$ as a $CO_2$ sink is not significant at loading below 0.4 mol $CO_2$/mol alkalinity. For 6 m AEP, free AEP is depleted at α = 0.3 mol/mol alkalinity. AEPH$^{+}$, AEPCOO$^{-}$, and $^{-}$OOCAEP are the three major products in the lean loading range. As $CO_2$ loading increases to α = 0.35, the amount of AEP(H$^{+}$)$_2$, H$^{+}$AEPCOO$^{-}$, $^{-}$OOCAEPH$^{+}$, and AEP(COO$^{-}$)$_2$ is more and more significant. At α above 0.35, AEP(H$^{+}$)$_2$ and H$^{+}$AEP(COO$^{-}$)$_2$ are the two dominant species, followed by $HCO_3^{-}$. (H$^{+}$)$_2$AEPCOO$^{-}$, $CO_3^{2-}$, and free $CO_2$ are not significant species in the solution across the entire $CO_2$ loading range.

Heat of absorption for 6 m AEP and 5 m PZ/2 m AEP decreases with $CO_2$ loading, due to the production of $HCO_3^{-}$ at rich loading. At 40 °C the heat of absorption of 6 m AEP is about 50–70 kJ/mol $CO_2$ at operation loading range (0.255–0.325) and the heat of absorption of 5 m PZ/2 m AEP is around 75–85 kJ/mol $CO_2$ at operation loading range (0.288–0.380).

## Acknowledgements

The authors acknowledge the financial support of the Texas Carbon Management Program.

The authors declare the following competing financial interest(s): One author of this publication consults for Southern Company and for Neumann Systems Group on the development of amine scrubbing technology. The terms of this arrangement have been reviewed and approved by the University of Texas at Austin in accordance with its policy on objectivity in research. The authors have financial interests in intellectual property owned by the University of Texas that includes ideas reported in this paper.

## References

[1] Rochelle GT. Amine Scrubbing for $CO_2$ Capture. Science 2009;325(5948):1652–54.

[2] Rochelle GT, Chen E, Freeman SA, Van Wagener DH, Xu Q, Voice AK. Aqueous piperazine as the new standard for $CO_2$ capture technology. Chem Eng J 2011;171(3):725–33.

[3] Freeman SA, Dugas RE, Van Wagener DH, Nguyen T, Rochelle GT. Carbon dioxide capture with concentrated, aqueous piperazine. Int J Greenh Gas Con 2010;4(2):119–24.

[4] Du Y, Li L, Namjoshi O, Voice AK., Fine NA., Rochelle GT. Aqueous Piperazine/N-(2-Aminoethyl) Piperazine for $CO_2$ Capture. Energy Proc 2013; 37: 1621–38.

[5] Austgen DM. A Model of Vapor-Liquid Equilibria for Acid Gas-Alkanolamine-Water Systems. The University of Texas at Austin. Ph.D. Dissertation. 1989.

[6] Chen C.-C, Bokis CP, and Mathias PM. A Segment-Based Excess Gibbs Energy Model for Aqueous Organic Electrolyte Systems. AIChE J 2001;47:2593.

[7] Posey ML. Thermodynamic Model for Acid Gas Loaded Aqueous Alkanolamine Solutions. The University of Texas at Austin. Ph. D. Dissertation. 1996.

[8] Hilliard MD. A Predictive Thermodynamic Model for an Aqueous Blend of Potassium Carbonate, Piperazine, and Monoethanolamine for Carbon Dioxide Capture from Flue Gas. The University of Texas at Austin, Austin, TX, 2008.

[9] Frailie PT, Plaza JM. Modeling piperazine thermodynamics. Energy Proc 2011;4:35–42.

[10] Pagano JM, Goldberg DE, Fernelius WC. A Thermodynamic study of homopiperazine, piperazine, and N-(2-aminoethyl)-piperazine and their complexes with copper(II) ion. J Phys Chem 1961;65:1062–64.

[11] Brelvi SW, O'Connell JP. Corresponding States Correlations for Liquid Compressibility and Partial Molar Volumes of Gases at Infinite Dilution in Liquids. AIChE J 1972:18:1239–43.

[12] Nguyen T. Amine Volatility in $CO_2$ Capture. The University of Texas at Austin. Ph. D. Dissertation. 2013.

[13] Chen X, Rochelle GT. Aqueous piperazine derivatives for $CO_2$ capture: Accurate screening by a wetted wall column. Chem Eng Res Des 2011;89(9):1693–710.